10-4-2018

A Parametric Study of Wave Interaction With a Rotor Having Hydrofoil Blades

Yingchen Yang

Fredrick A. Jenet

Ben Xu

Juan Carlos Garza

Benjamin Tamayo

See next page for additional authors

Authors

Yingchen Yang, Fredrick A. Jenet, Ben Xu, Juan Carlos Garza, Benjamin Tamayo, Yessica Chavez, Oscar Reyes, and Samuel Fuentes

Proceedings of the ASME 2018 Power Conference
POWER2018
June 24-28, 2018, Lake Buena Vista, FL, USA

POWER2018-7391

A PARAMETRIC STUDY OF WAVE INTERACTION WITH A ROTOR HAVING HYDROFOIL BLADES

Yingchen Yang*, Fredrick Jenet, Ben Xu
University of Texas Rio Grande Valley, Brownsville·Harlingen·Edinburg, Texas, USA

Juan Carlos Garza, Benjamin Tamayo, Yessica Chavez, Oscar Reyes, Samuel Fuentes
Instituto Tecnológico de Matamoros, Matamoros, Mexico

ABSTRACT

Our recent progress on studying wave interaction with a lift-type rotor is discussed in this paper. The particular focus is on characterization of the rotor's unidirectional responsiveness in waves. The rotor consists of six hydrofoil blades in two sets. One blade set has three blades laid out as a vertical-axis wind turbine of the Darrieus type. The other blade set has three blades configured like a Wells turbine. In combination, the formed rotor can be driven by flows in any direction to perform unidirectional rotation about its vertically mounted shaft. This unidirectional responsiveness of the rotor also holds in waves, making the rotor a valuable device for wave energy conversion. For parametric study of the rotor, hydrofoil blades using different cross sectional profiles and chord lengths have been employed to configure the rotor. The rotor was then tested in a wave flume under various wave conditions in a freewheeling mode. Experimental results were analyzed and discussed. The yielded research findings will greatly enhance the fundamental understanding on the rotor performance in waves, and effectively guide the prototype rotor development for practical applications.

Key words: wave energy converter, WEC, vertical axis, unidirectional rotor.

* Address all correspondence to this author. Email: yingchen.yang@utrgv.edu

1. INTRODUCTION

Energy harvesting from waves, winds, and tides/currents can essentially be considered as energy extraction from fluid flows. Specifically, energy harvesting devices are employed to absorb kinetic energy from the fluid flows and convert it into electricity. In the case of winds and tides/currents, incoming flow conditions are rather simple: the devices see relatively steady flows (with turbulence). For this reason, wind turbines and hydrokinetic turbines share quite similar, if not exactly the same, technologies and working principles [1]. And, flow interaction with the two types of turbines exhibits similar flow physics. In the case of waves, however, the flow is unsteady and omnidirectional due to the orbital motion of water particles, the Stokes drift, and the superposition of different wave frequency components [2, 3]. Such a complex flow nature makes energy harvesting from waves much more difficult and less efficient than from steady flows.

A wave energy converter (WEC) is a device that absorbs hydrokinetic energy from ocean waves and converts it into electricity. WECs can be categorized into a reciprocating class and a unidirectional class according to the motion type [4]. The reciprocating class is overly dominant; specific motions include heaving up and down, swaying/rocking/pitching back and forth, periodic bending/curving, and more [5]. The unidirectional class is rather rare; the WECs perform unidirectional rotation either about a horizontal axis [6] or a vertical axis [7].

Reciprocating WECs rely on the resonance principle to achieve a nominally high efficiency. Their main drawback is that the reciprocating WECs are frequency-specific. Energy transfer in reciprocating WECs can go to two extremities solely based on the changing wave frequency. With a good match between the dominant wave frequency and a reciprocating WEC's resonant frequency, an optimal phase relation between the wave motion and WEC motion is reached and maintained, and water flow in waves constantly feeds energy to the WEC, leading to the resonance and high efficiency. With a mismatch in frequencies, however, the optimal phase relation no longer exists and strong energy transfer occurs in both ways, resulting in a suppressed WEC motion and poor efficiency.

Unidirectional WECs, on the other hand, respond well to a wide range of wave frequencies since they do not use the resonance principle. Furthermore, vertical-axis unidirectional WECs are advantageous over horizontal-axis ones due to their tolerance to the wave propagation direction [8]. Vertical-axis unidirectional WECs can further bypass the need for a yaw mechanism that is employed in many reciprocating WECs and horizontal-axis unidirectional WECs to realigning them with the changing wave propagation direction. Overall, the vertical-axis unidirectional WECs demonstrate a great potential as an effective means to harvest wave energy at a low cost.

In this paper, a new vertical-axis unidirectional WEC is presented. It is essentially a lift-type vertical-axis rotor in a hybrid structure of a Darrieus-type vertical-axis wind turbine [9] and a Wells turbine [10]. The Darrieus turbine structure enables the rotor for unidirectional rotation in horizontal flows, whereas the Wells turbine structure makes the rotor perform unidirectional rotation in vertical flows. Upon integration of the two structures in one rotor, it can be driven by flows in any direction to perform unidirectional rotation about its vertically mounted shaft. This unique feature is well suited for wave energy conversion. The objective of the present research is to characterize this vertical-axis unidirectional rotor's performance through parametric study by experimental means.

2. EXPERIMENTAL SYSTEM

Water particles in waves perform orbital motion in a vertical plane with Stokes drift [2]. To simulate wave interaction with a vertical-axis rotor under certain simplified conditions, the rotor was translated in quiescent water in a wave flume along a circular path in a vertical plane. Such circular motion approximates simple deep waves by neglecting the Stokes drift. The wave flume has inner dimensions of 15m (L) × 1m (W) × 1.3m (H). To further characterize the rotor's unidirectional responsiveness to omnidirectional flows, horizontal and vertical oscillations of the rotor in quiescent water were also carried out. The diameter for the circular path and the peak-to-peak amplitude for the horizontal and vertical oscillations represent the wave height H, and the frequency of each motion represents the wave frequency f_W. A servo-motor-driven translational carriage to realize these three types of the rotor motion was built in house [8]. The three types of the rotor motion are termed as the carrying motion in this paper.

A typical lift-type vertical-axis rotor employed in this study is shown in Fig.1. It consists of six blades of hydrofoil cross sections with a constant chord length along a straight span. The six blades are evenly distributed around a vertical shaft in two sets. One set has three vertical blades to drive the rotor in horizontal flows. The other set has three horizontal blades to drive the rotor in vertical flows. When the rotor rotates about the fixed shaft, it forms a circular swept area of diameter D, which is defined as the rotor diameter. For all the experiments discussed in this paper, the rotor diameter was fixed at D = 500 mm. In addition, the span S for all the individual blades was fixed at S/D = 0.257, the spoke-to-spoke distance L between the two blade sets along the shaft direction was fixed at L/D = 0.3, and the simulated wave height was fixed at H/D = 0.635.

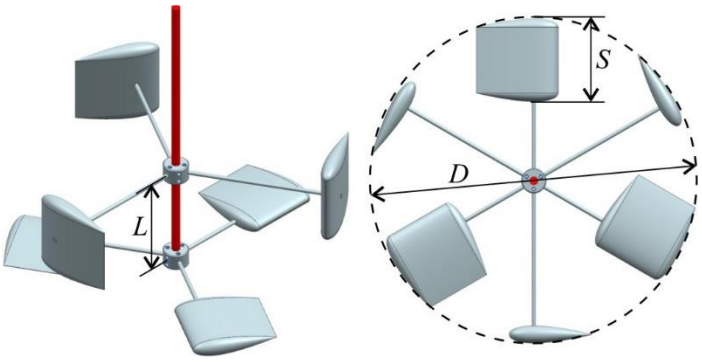

(a) Perspective view (b) Top view

Figure 1: A typical lift-type rotor configuration.

Other than the fixed parameters as specified above, more parameters were varied for parametric study. Fig. 2 shows four hydrofoils employed in making different rotor blades. The parameter C is for the chord length of a hydrofoil. Note that NACA0021 and NACA0021-cambered have the same chordwise thickness distribution, but NACA0021-cambered has an arc camber line of radius R = 0.5D. All the blades were 3D-printed, polished, and painted before constructing rotors for

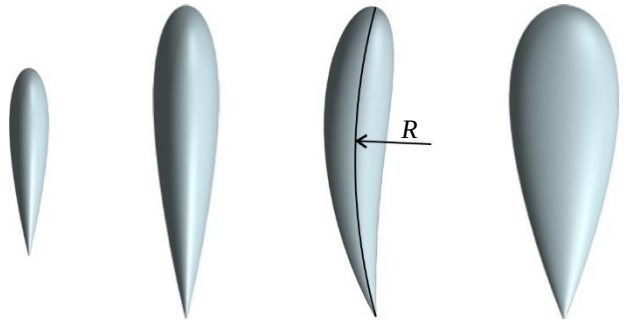

NACA0021 C = 76 mm | NACA0021 C = 127 mm | NACA0021-cambered C = 127 mm | NACA0035 C = 127 mm

Figure 2: Comparison of hydrofoils employed.

testing. The rotors were tested at different values of the simulated wave frequency, f_W = 0.333, 0.5, 0.667, and 0.833 Hz.

With a rotor mounted to the translational carriage through a shaft-bearing-housing mechanism, the rotor can freely rotate about its shaft at low friction with no power takeoff. This condition is termed as freewheeling. The focus of the present research is on characterizing the rotor's unidirectional rotation behavior about the vertical shaft in freewheeling mode. Under various testing conditions, time traces of the rotor's angular velocity were obtained at a sample rate of 30 samples per second for approximately 75 seconds per run. Three repetitive runs were conducted in each testing condition for calculating the averaged angular velocity and the standard deviation. In presenting the averaged angular velocity throughout the paper, no error bars were included due to the very small values of the standard deviation. The detailed procedure for data acquisition and processing were discussed in one of our earlier papers [8].

3. RESULTS AND DISCUSSION

Employing the blade layout as shown in Fig. 1 with six identical blades having a NACA0021 cross section and a chord length of 127 mm, a basic rotor was configured and tested first. Upon characterization of this basic rotor under specified conditions, other rotors of various blade dimensions and configurations were compared with it for the parametric study.

Fig. 3 compares the time traces of the rotor's angular velocity about its vertical shaft in three carrying motion types – circular motion, horizontal oscillation, and vertical oscillation. Regardless of different carrying motions, all the time traces demonstrate unidirectional angular velocity with fluctuation. Yet, the averaged angular velocities and fluctuation levels are quite different. Specifically, the circular motion (Fig. 3a) and vertical oscillation (Fig. 3c) enable mush stronger averaged angular velocities than the horizontal oscillation (Fig. 3b), but the horizontal one (Fig. 3b) presents much less fluctuation than the other two (Figs. 3a and 3c). It is noteworthy that both time traces for the horizontal and vertical oscillations (Figs. 3b and 3c) are similar to a rectified and shifted sinusoidal signal. This is due to the fact that rotor responses to opposite flows in every oscillation cycle repeat to a large extent. A noticeable high-low alternating pattern rather than a relatively even distribution of the top peaks are observed in the time trace for the vertical oscillation though (Fig. 3c). This is attributed to the top-to-bottom asymmetry of the rotor configuration – with the top three blades being vertical and three bottom ones horizontal (Fig. 1a). In Fig. 3c, the high top peaks are associated with downstrokes and the low top peaks with upstrokes. With the rotor's circular carrying motion in a vertical plane closely simulates simple deep waves, the associated time trace of the angular velocity (Fig. 3a) is more complex than that in vertical and horizontal oscillations (Figs. 3b and 3c). In each period of the circular translation, the rotor passes through the highest and lowest points with the strongest horizontal motion and the leftmost and rightmost points with the strongest vertical motion. Reflected on the time

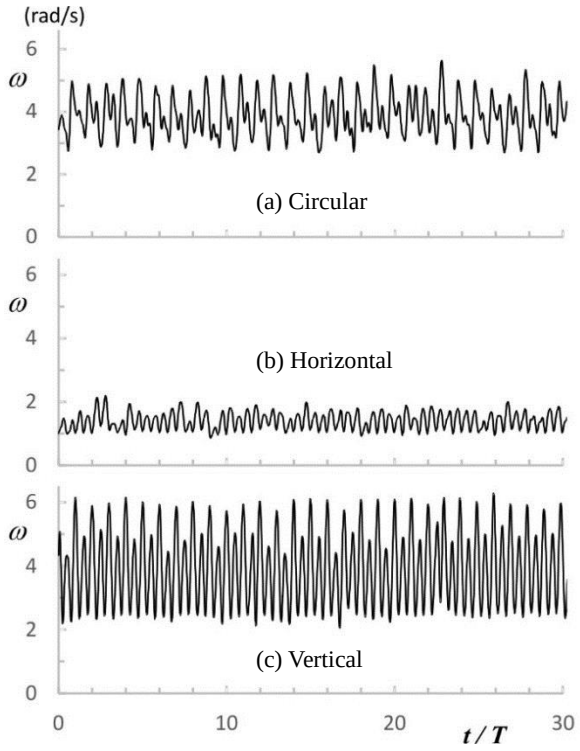

Figure 3: Angular velocity ω versus normalized time t/T (T being the period) for the basic rotor in three carrying motion types. The simulated wave frequency is fixed at f_W = 0.667 Hz.

trace in Fig. 3a, in each period of the circular carrying motion there are two top peaks with the strongest horizontal motion and two bottom peaks with the strongest vertical motion. The relatively weak rotor response to the horizontal flow can be remedied by changing the shape and/or dimensions of the three vertical blades in Fig. 1.

The amplitude spectra associated with the time traces of the angular velocity in Fig. 3 are shown in Fig. 4. It is evident that, in all the three cases considered, there is a dominant peak at two times of the simulated wave frequency, f/f_W = 2. This is consistent with the earlier discussion on the time traces, since the rotor responses to two opposite flows in each cycle repeat to a large extent. The non-repeating component is reflected by a less dominant peak at f/f_W = 1 in the circular and vertical cases, where the rotor has an asymmetrical top-to-bottom configuration (Fig. 1) and leads to a periodic response at the wave frequency only. In comparison, the symmetric left-to-right rotor configuration guarantees well repeated rotor responses to horizontal opposite flows. Therefore, for the horizontal case in Fig. 4, no peak at f/f_W = 1 is detected. For all the cases in Fig. 4, higher harmonics are hardly noticeable.

To examine the performance of the basic rotor in a range of the simulated wave frequency f_W, averaged angular velocity $\overline{\omega}$ were plotted against f_W and compared among the three carrying motion types, as shown in Fig. 5. It is intuitive that at a fixed wave height and with increasing f_W, $\overline{\omega}$ increases in general. In

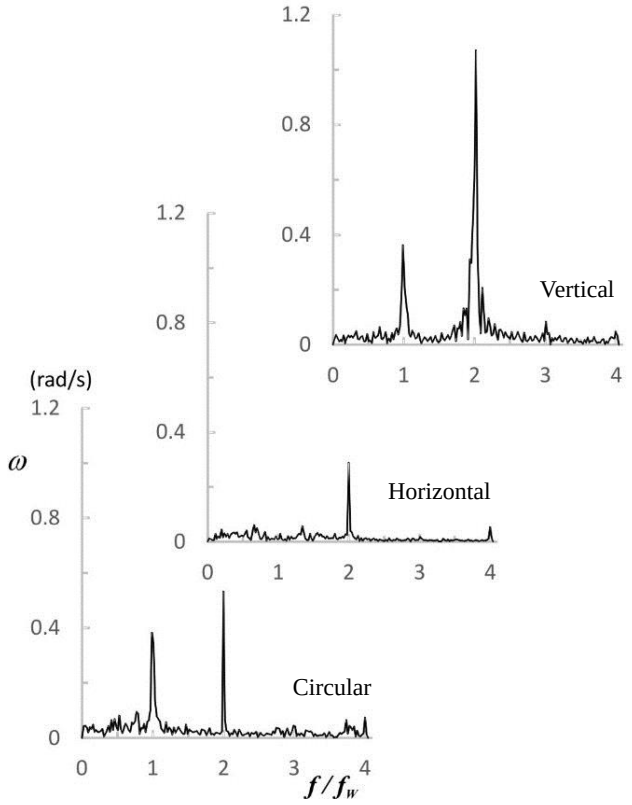

Figure 4: Amplitude spectra for the time traces of the angular velocity in Fig. 3.

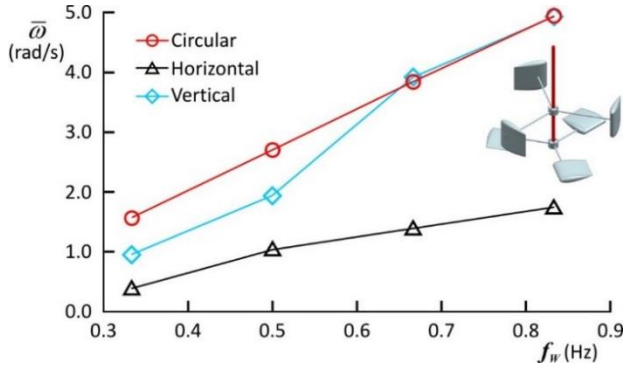

Figure 5: Averaged angular velocity $\overline{\omega}$ versus the simulated wave frequency f_W for the basic rotor in three carrying motion types.

the lower range of f_W, the circular case has the highest value of $\overline{\omega}$, followed by the vertical case in the middle and the horizontal case at the bottom. In the upper range of f_W, however, the vertical case is as strong as the circular one, and both of them are far above the horizontal case.

Based on the basic rotor design, two more rotors were constructed and tested under the same conditions as for the basic rotor. In one rotor design, the six identical blades employed the same hydrofoil profile as in the basic rotor – NACA0021, but the chord length was reduced from C = 127 mm for the basic rotor to C = 76 mm. In another rotor design, the six identical blades had a thicker hydrofoil profile NACA0035 but with the same chord length C = 127 mm compared to the basic rotor. For a direct comparison, the averaged angular velocity $\overline{\omega}$ for these three rotors in the three carrying motion types are jointly presented in Fig. 6. For the two new rotors, however, the tested frequency range was reduced by removing the high frequency 0.833Hz due to the strength consideration of the 3D-printed plastic blades.

As shown in Figs. 6a through 6c and in comparison with the basic rotor, a reduced chord length C led to a remarkably reduced $\overline{\omega}$ in all the three carrying motion types. On the other hand, an increased blade thickness only caused very little change in $\overline{\omega}$,

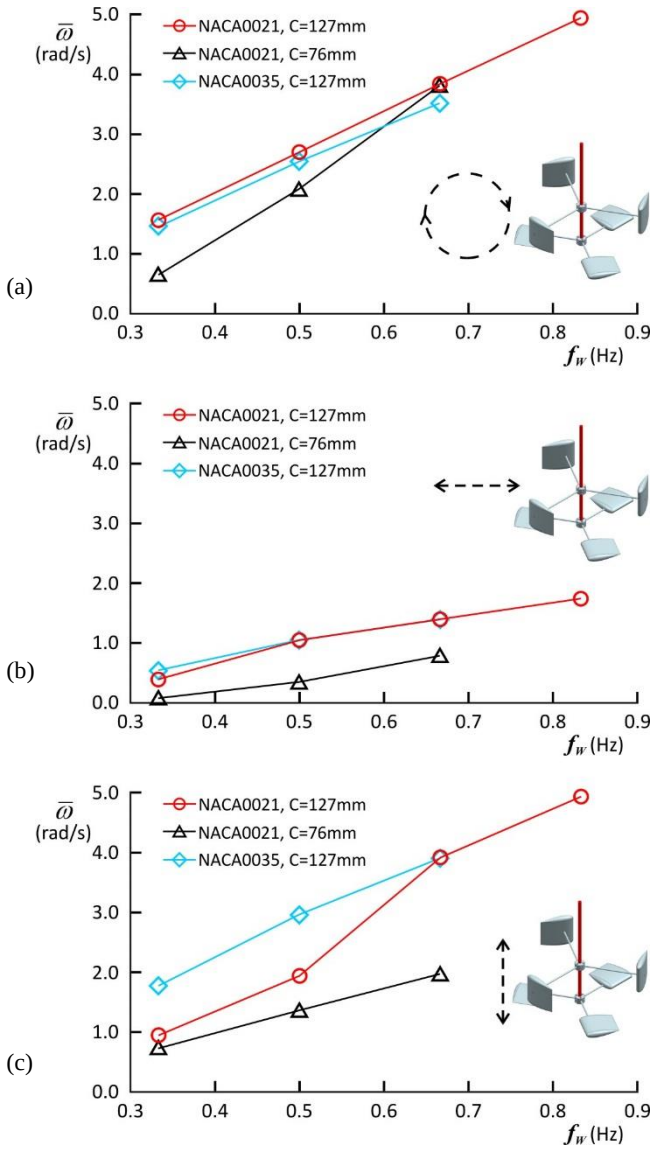

Figure 6: Comparison of $\overline{\omega}$ versus f_W among three rotors in three carrying motion types. (a) Circular motion. (b) Horizontal oscillation. (c) Vertical oscillation.

except for the vertical case in the lower frequency range where a significant increase in $\overline{\omega}$ is observed.

In an effort to explore the blades' camber effects on the rotor performance, three NACA0021-cambered blades (Fig. 2) were employed to replace the three vertical NACA 0021 blades in the basic rotor to form a modified basic rotor. On this modified rotor, the three horizontal NACA0021 blades from the basic rotor were reused. As shown in Fig. 7 and in comparison with Fig. 5, the usage of the three cambered vertical blades greatly increased $\overline{\omega}$ under all the testing conditions. Undoubtedly, this modified basic rotor demonstrates a very promising potential.

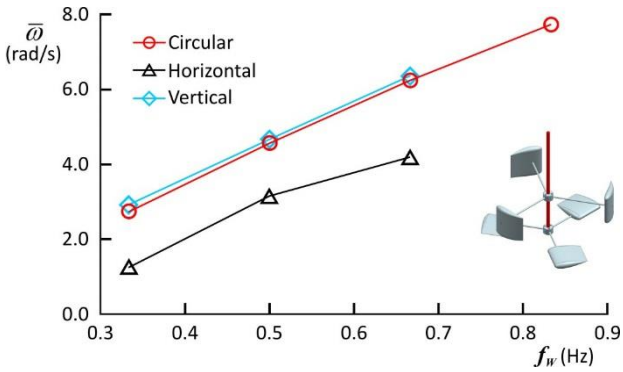

Figure 7: Averaged angular velocity $\overline{\omega}$ versus the wave frequency f_W for the modified basic rotor in three carrying motion types.

To better characterize the camber effects, comparison between two partial rotors were made in Fig. 8. One partial rotor has three vertical NACA0021 blades only and the other three vertical NACA0021-cambered blades only. In circular motions as shown in Fig. 8, the partial rotor with cambered blades run nearly twice as fast as the one with symmetric blades. It is evident that the cambering of the blades has greatly reduced the drag during the rotor's rotation.

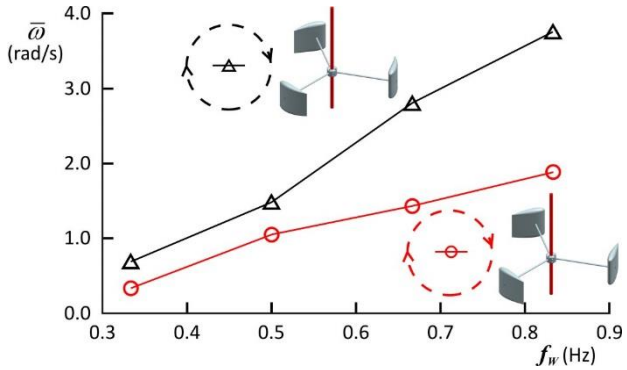

Figure 8: Comparison of $\overline{\omega}$ versus f_W between two partial rotors with one having cambered blades and the other symmetrical blades.

In general, the modified basic rotor are advantageous over others in performing unidirectional rotation about the vertical shaft in freewheeling mode in simulated simple deep waves. For an extended characterization to gain in-depth understanding, the modified basic rotor were further tested in components, as illustrated in Fig. 9. Specifically, Figs. 9a through 9d show time traces of the angular velocity for the rotor having one horizontal NACA0021 blade in vertical oscillation, three horizontal NACA0021 blades in vertical oscillation, one vertical NACA0021-cambered blade in horizontal oscillation, and three vertical NACA0021-cambered blades in horizontal oscillation, respectively. The overall impression on Fig. 9 is that, unidirectional rotation with fluctuation was achieved in all the above specified testing conditions, including the single-blade rotors. It is very interesting that, a single-blade rotor did as well as, or even slightly better than, a three-blade rotor under the same testing conditions in the freewheeling mode. Nonetheless, it does not by any means imply the same rotor behavior in a power-takeoff mode where a resistive load is applied.

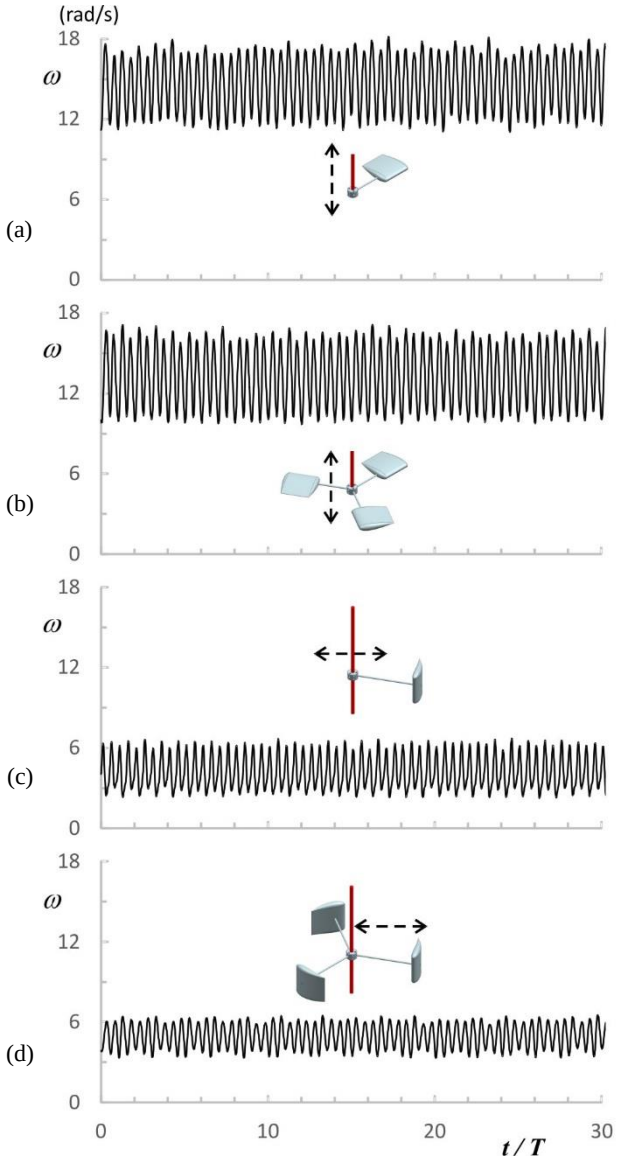

Figure 9: Time traces with different blade layouts and in different types of the carrying motion at f_W = 0.667 Hz.

Fig. 10 shows the amplitude spectra of the time traces in Fig. 9. For all the four cases presented, there is an overly dominant peak at $f/f_W = 2$. In contrast, at $f/f_W = 1$ a much weakened peak, if not completely vanished, exists in most cases due to the top-to-bottom and left-to-right symmetry (while rotating). All the spectra demonstrate a very clean background, making the higher harmonics discernable.

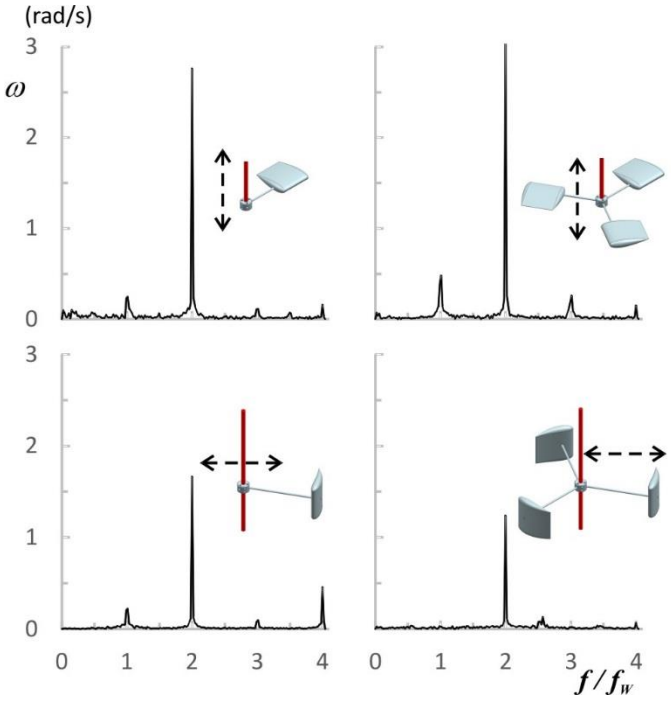

Figure 10: Amplitude spectra associated with time traces in Fig. 9.

More testing results on the modified basic rotor in components are presented in Fig. 11 in the form of the averaged angular velocity $\overline{\omega}$ versus the wave frequency f_W. In the case of a rotor with horizontal blade(s) in vertical oscillation, one blade generates a slightly higher value of $\overline{\omega}$ than three blades. In the case of a rotor with vertical blade(s) in horizontal oscillation, it is the other way around.

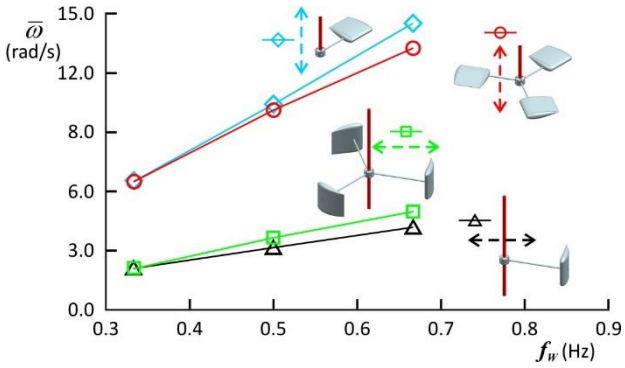

Figure 11: Comparison of $\overline{\omega}$ versus f_W among four blade layouts in two types of the carrying motion.

4. CONCLUSIONS

A vertical-axis lift-type rotor was constructed and tested in simulated waves under a freewheeling condition. It consisted of two sets of blades with hydrofoil cross sections. One set was responsive to horizontal flows and the other to vertical flows. The joint effect of the two sets of blades made the rotor perform unidirectional rotation about a vertical axis when exposed in waves. The rotor performance was characterized in terms of the angular velocity by varying the shape and size of individual blades of a complete rotor, by dealing with a partial rotor with a single blade set or even a single blade, and by changing the simulated wave frequency in a certain range. The testing results demonstrated a promising rotor that performed profound unidirectional rotation very consistently under all the explored conditions. The rotor can enable a simple yet efficient wave energy converter to harvest energy from ocean waves.

REFERENCES

[1] M.S. Guney and K. Kaygusuz, "Hydrokinetic energy conversion system: A technology status review," *Renewable and Sustainable Energy Reviews*, **14** (9), 2996-3004, 2010.

[2] G. L. Pickard and S. Pond, "Introductory Dynamical Oceanography (2nd ed.)," Butterworth-Heinemann, 1983.

[3] O. M. Phillips, "The dynamics of the upper ocean (2nd ed.)," Cambridge University Press, 1977.

[4] Y. Yang, "Unidirectional rotary tendency of a wave-driven rotor," *Journal of Energy and Power Engineering*, **8**, 1607-1619, 2014.

[5] I. López, J. Andreu, S. Ceballos, I. M. de Alegría, and I. Kortabarria," Review of wave energy technologies and the necessary power-equipment," *Renewable and Sustainable Energy Reviews*, **27** , 413-434, 2013.

[6] M. R. Ahmed, M. Faizal, and Y. H. Lee, "Optimization of blade curvature and inter-rotor spacing of Savonius rotors for maximum wave energy extraction," *Ocean Engineering*, 65, 32-38, 2013.

[7] E. A. Rossen, P. C. Scheijgrond, and R. Mikkelsen, "Development and model test of a combined Wells-Darrieus wave rotor," in *Proceedings of 4th European wave Energy Conference*, Aalborg University, Denmark, 2000.

[8] Y. Yang, F. Salazar, and J. Soto, "A vertical axis rotor for wave energy conversion," *ASME 2017 Fluids Engineering Summer Conference*, Waikoloa, Hawaii, Jul 30-Aug 3, 2017.

[9] M.H. Mohamed, "Performance investigation of H-rotor Darrieus turbine with new airfoil shapes," *Energy*, **47**, 522-530, 2012.

[10] S. Raghunathan, "The Wells air turbine for wave energy conversion," *Progress in Aerospace Sciences*, 31, 335-386, 1995.